DESIGN AND SIMULATION OF SUPERSONIC PROFILING NOZZLE FOR U78CRV RAIL HEAT TREATMENT

Huizeying Zhang, Mingxin Gao*, Lincong Xu, Yang Wang

School of Mechanical Engineering and Automation, University of Science and Technology Liaoning, Anshan 114051, Liaoning, China

* Corresponding author; E-mail：gaoming31@163.com

In order to address with the defects of poor cooling capacity and cooling uniformity of the rail air-quenching technology, the supersonic profiling nozzle (SP nozzle) was designed to improve the cooling capacity through supersonic jet and improve the cooling uniformity through the profiling structure of the rail head. Numerical simulation method combined with experimental were used to study the heat transfer characteristics of SP nozzle on rail. The results showed that air-cooled quenching at a pressure of 0.4 MPa increased the cooling capacity of the SP nozzle by 23.96%, 15.35% and 31.69%, and the cooling uniformity by 36.82%, 46.98% and 22.19% over the existing circular normal nozzle, circular supersonic nozzle and normal profiling nozzle, respectively. A segmented cooling process curve of "slow first and then fast" was designed, and the cooling time of the segmented cooling SP nozzle was shortened by 49s compared with the CR nozzle. Compared to the SP nozzle cooled at a constant rate, the cooling time is shortened by 35 seconds. Regulate the inlet pressure of the SP nozzle to cool the rail at a cooling rate close to but not exceeding the critical cooling rate of pearlite transformation before the rail temperature is lower than the end temperature of pearlite transformation (about 500 ℃), and then increase the inlet pressure as much as possible, which is beneficial to improve the production efficiency on the premise of ensuring the performance of the heat-treated rail.

Keywords： *rail; heat treatment; supersonic profiling nozzle; heat exchange characteristics*

1. Introduction

Rail is a critical component of railway infrastructure, bearing the full load of train operations. The shift toward high-speed, heavy-duty railways and high-density transportation demands improved rail performance

[1]. In China, the 75 kg/m pearlitic rail represents the latest in high-strength rail technology, currently utilized on heavy-duty routes such as the Da-Qin and Shuo-Huang railways [2]. The under-velocity air-cooled quenching process is a heat treatment method where compressed air is sprayed onto the rail surface via nozzles, accelerating cooling to achieve a lamellar pearlite structure, without forming martensite or bainite [3]. This process is key to enhancing rail strength and toughness. At present, the air-cooled quenching technique relies on three circular nozzles to cool the rail head from the top and sides. However, this setup presents significant limitations in cooling capacity and uniformity. For example, in the case of U78CrV rail, the critical cooling rate for heat treatment ranges between 3-6°C/s, while the current nozzle setup only achieves about 1-2°C/s, which restricts further process optimization [4-6]. Additionally, the distance between nozzle outlets and the rail surface impacts heat transfer, with variations in nozzle positioning causing uneven cooling rates across the rail head cross-section. The area directly beneath the nozzle cools faster than other sections [7-8].

To address these challenges, researchers have pursued improvements in both cooling capacity and uniformity. In one approach, Song, L., [9] designed a circular supersonic nozzle with the same cross-sectional area and arrangement as current production nozzles, achieving a significant boost in cooling capacity. However, the localized cooling enhancement compromised overall uniformity. In a separate effort focused on cooling uniformity, Li, X., et al. [10] developed a cap-shaped air jet with smaller apertures tailored to the rail head's shape, while Li, D., et al. [11] created a rectangular air outlet with a circular profile. Shan, Z., [12] designed a profiling flat slit nozzle, which significantly improved uniformity across different rail sections. Although each approach has had success in either cooling capacity or uniformity, few have managed to optimize both aspects. Kang, H., [13] developed a circular supersonic nozzle with small apertures closely arranged on an air jet head with a trough structure, which improved both capacity and uniformity. However, this design included 517 air outlets along a 500 mm length, generating considerable air friction along the nozzle walls and somewhat reducing heat exchange efficiency. A promising solution would combine the high cooling capacity of supersonic jets with the uniform cooling offered by profiling nozzles, potentially overcoming the limitations of current rail quenching processes.

The supersonic nozzle consists of a subsonic contraction section, a throat, and a supersonic expansion section [14]. Its operation is as follows: as compressed air enters the contraction section, the velocity increases due to a decreasing cross-sectional area. At the throat, the air flow reaches local sound speed; beyond the throat, in the expansion section, the cross-sectional area gradually widens, allowing further air flow expansion and acceleration, ultimately producing a supersonic jet [15]. The design ratio of these sections is constrained by the desired outlet flow rate and inlet pressure.

Given the rail head’s unique shape, achieving a uniform supersonic jet with conventional profiling designs based on simple equidistant transformations proves difficult. In a standard supersonic nozzle, the throat’s cross-sectional area should be smaller than that of the expansion section’s outlet; however, equidistant profiling often results in a throat cross-section larger than the outlet. This paper presents the design of a rail-specific

supersonic profiling nozzle (SP nozzle) with a three-chamber structure that balances cooling capacity with cooling uniformity. Heat exchange characteristics were examined through numerical simulations and experimental analysis.

2. SP nozzle structure design

2.1. Design Method

The main design parameters of the SP nozzle are shown in Fig. 1, including the height of the shrinking section $A1$, the height of the throat $A2$, the height of the expansion section $A3$, the inlet width of the shrinking section $B1$, the throat width $B2$, the outlet width of the expansion section $B3$, the inlet length of the shrinking section $L1$, the length of the throat center $L2$, the length of the outlet $L3$, the length of the straight section of the side outlet $L4$, the angle between the straight section of the side outlet and the wall surface of the outlet $a3$, the angle of the shrinking section $a1$, the angle of the expansion section $a2$, and the jet height H. The design method and process of the SP nozzle are as follows:

(1) The top and both sides of the rail head section are used as the design reference for the outlet and throat profile curve of the SP nozzle expansion section. The rail head curve is transformed at an equidistant scale according to the jet height H to obtain the shape of the $L3$ curve. Correspondingly, the rail head curve is converted equidistantly according to $H+A3+0.5A2$ to obtain the shape of the $L2$ curve.

(2) The calculation of the throat cross-sectional area $S2$ of the nozzle is carried out according to the requirements: in order to ensure comparability, the same throat cross-sectional area as the existing nozzle (the smallest cross-sectional area of the nozzle) is selected in this paper.

(3) Outlet cross-sectional area $S3$ design for the expansion section: according to the jet velocity and $S2$ requirements, the outlet cross-sectional area $S3$ is calculated using the following formula.

$$S3 = B3 \times L3 = \frac{S2}{Ma}\left[\left(\frac{1}{k+1}\right)\left(1+\frac{k-1}{2}\times Ma^2\right)\right]^{\frac{k+1}{2(k-1)}} \tag{1}$$

Where K is the specific volume ratio of gas and Ma is the design Mach number of the jet velocity at the nozzle outlet.

(4) Jet height H, throat width $B2$, and throat center curve length $L2$ design: due to the long and narrow profile of the profiled nozzle, in order to reduce the influence of friction resistance between air and the nozzle wall, the throat width $B2$ should not be too small, generally not less than 0.5 mm. Additionally, the distance between the actual produced rail and the nozzle outlet should not be too close, generally not less than 4 mm. Based on the identified H, $B2$, and $S2$, $L2=S2/B2$ can be calculated.

(5) Throat height $A2$ design: In order to stabilize the airflow, $A2$ should be greater than $B2$ and less than three times $B2$, i.e.:

$$3B2 > A2 > B2 \tag{2}$$

(6) Designing the nozzle side outlet straight-line section $L4$, the outlet wall angle $a3$, the expansion section height $A3$, the expansion section outlet width $B3$, and the expansion section outlet curve length $L3$: $L3$ contains the middle curve section $L3c$ and the two sides of the straight-line section $L4$, namely:

$$L3 = L3c + 2L4 \tag{3}$$

Given that:

$$L3c = 2(L5 + 2\pi H\frac{a4}{360}) + 2(L6 + 2\pi H\frac{a5}{360}) + (L7 + 2\pi H\frac{a6}{360}) \tag{4}$$

With $a4$, $a5$ and $a6$ representing the arc lengths of each arc section of the rail head, and $L5$, $L6$ and $L7$ are the arc lengths of each arc section of the rail head (as shown in Figure 1).

The laryngeal center curve $L2$ is calculated as follows:

$$L2 = L2c + 2L2s \tag{5}$$

Among them: $L2c$ and $L2s$ are the lengths of the curve segment and the lengths of the straight segments on both sides of $L2$, respectively.

$$\begin{aligned} L2c = {} & 2[L5 + 2\pi(H + 0.5A2 + A3)\frac{a4}{360}] + 2[L6 + 2\pi(H + 0.5A2 + A3)\frac{a5}{360}] \\ & + [L7 + 2\pi(H + 0.5A2 + A3)\frac{a6}{360}] \end{aligned} \tag{6}$$

The relationship between $L2s$ and $L4$ is as follows:

$$L4 = L2s + \frac{A3 + 0.5A2}{\tan(a3)} \tag{7}$$

Constraint 1: In order to ensure the cooling effect on the side of the rail head, $L2s$ should not be less than zero.

Constraint 2: In the selection of angle $a3$, the line extension from the lower end of the straight line $L2s$ to the lower end of $L4$ should be lower than the lower end of the straight line on the side of the rail head. Namely:

$$a3 \le \arctan(\frac{0.5A2 + A3 + H}{L8 - L2s}) \tag{8}$$

Given that $L8$ is the length of the straight segment on the side of the rail head.

Constraint 3: Both $A3$ and $a3$ will affect the aspect ratio of each section of the nozzle, which in turn will affect the flow field of the jet and ultimately the heat transfer capacity. For example, the smaller the $A3$ value, the smaller the $L2c$, and the greater the $B2$ at the same cross-sectional area. For example, when $L2c$ and $A3$ are determined, the larger the $a3$, the smaller the $L3$, and the larger the $B3$ at the same cross-sectional area. In order to ensure the effective heat exchange area of the nozzle in the width direction, $a2>0$, i.e., $B3>B2$.

(7) Inlet cross-sectional area design for the shrinking section $S1$, the length of the inlet curve $L1$ and the width $B1$: in order to stabilize the airflow, $S1$ should be greater than $S3$, and it is generally selected by 1.5-2 times, that is:

$$1.5S3 \le S1 = B1 \times L1 \le 2S3 \tag{9}$$

(8) Designing the height of the shrinkage section $A1$: When selecting $A1$, the angle of the shrinkage section $a1$ should be between 5-10°, that is:

$$\frac{B1-B2}{2\tan(30)} \le A1 \le \frac{B1-B2}{2\tan(15)} \tag{10}$$

(9) In order to ensure the cooling capacity of the side of the rail head, the nozzle after the designed parameters, is deformed into a three-cavity structure: the nozzle cavity is truncated along the parallel plane of the upper end of $L4$ and the nozzle outlet wall on the nozzle. The curve part of $L1$ and $L3$ of the cavity, after the two sides are truncated, becomes a straight line, and $a3$ becomes 90°. The cavity, after the two sides are cut off, is then moved down to the middle position of the side of the rail head. The final nozzle cavity is shown in Fig. 2.

(10) In order to reduce air resistance, the junction between the larynx and the contraction and expansion segments is smoothly transitioned.

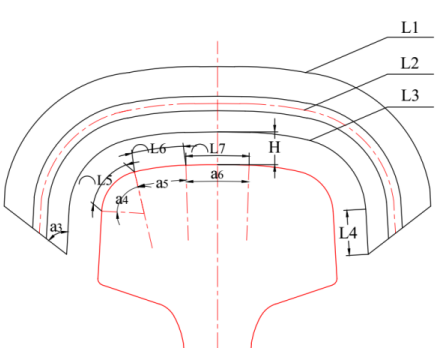

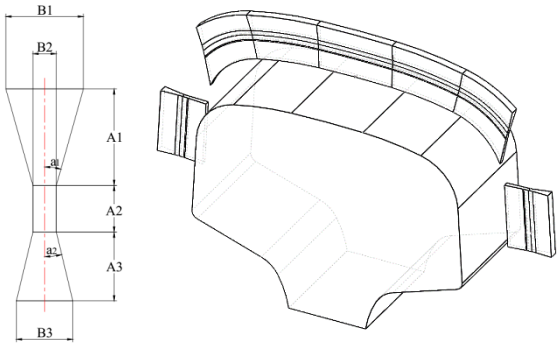

Fig. 1 Main design parameters of SP nozzle **Fig. 2 Schematic diagram of SP nozzle cavity structure**

2.2. SP nozzle parameter design

At present, the minimum diameter of the shrink nozzle used in production is 7mm, and the total cross-sectional area of the three nozzles in the same section of the rail head is 115.395mm^2. Therefore, the $S2$ of the SP nozzle is determined to be 115.395mm^2. According to 0.3MPa as the design inlet pressure and 1.35Ma as the design outlet Mach number, $S3$ is calculated to be 125.67mm^2 using Eq. (1). According to Ref. [8], the optimal jet height for the heat transfer capacity of the supersonic air jet is close to H/D=4; therefore, H=4mm and $B2$=0.95mm be selected, and the length of $L2$ is calculated as follows: $L2=S2/B2$=121.47mm. According to Eq. (2), the throat height $A2$ is 2mm. According to China's rail quality inspection standard "TB/T2344.1-2020," the size of the rail head curve section for 75 kg/m rail is: $L5$=20.30mm, $L6$=14.25mm, $L7$=1960mm, $a4$=78°, $a5$=10°, and $a6$=2°. Combined with Constraint 1 and Eqs. (3) – (7), $A3 \leqslant 5.44$mm is calculated. In the initial design, the value of $A3$ was set to 5mm. The actual value of $L8$ is 26.8mm, and Constraint 3 is not satisfied after calculation, so the length of $L8$ is taken as 23mm, resulting in $a3 \leqslant 24.23°$ according to Constraint 2. According to Eq. (4) and Eq. (7), $L3c$=101.12mm and $L4$=14.06mm. In this case,

$B3=S3/L3=0.97$mm, which satisfies the requirements of Constraint 3. According to Eq. (9), $S1=2S3=251.34$mm². Combined with Eq. (10), $A1=5$mm, resulting in $L1=117.61$mm and $B1=2$mm, at which point $a1=6°$, meeting the design requirements of 5-10°.

3. SP nozzle heat transfer characteristics

3.1. Numerical simulation model

At present, the spacing between two adjacent rows of nozzles along the length of the rail is 30mm [12]. Therefore, the rail length is selected as 30mm in the simulation, and axisymmetric boundary conditions are set on both end faces of the rail. The mesh is created using polyhedral elements. A boundary layer is established on the wall surface of the nozzle and the contact surface between the jet and the rail, with the number of layers set to 5, the size of the first layer being 0.005mm, and the transformation gradient set to 1.2. Due to the small cross-sectional width of the nozzle, the flow field near the nozzle cavity and nozzle outlet is partially refined to optimize calculation efficiency and mesh orthogonality. The divided mesh is shown in Fig. 3.

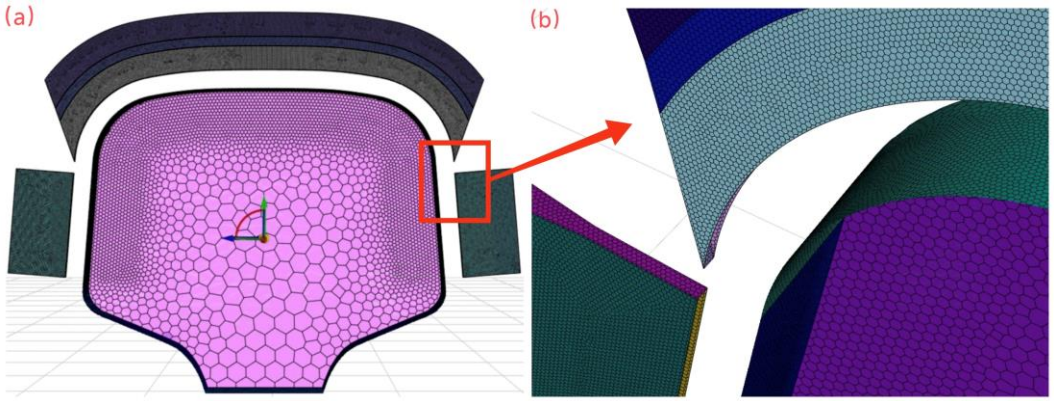

(a) Monolithic grid (b) Zoom in on the mesh locally

Fig. 3 3D simulation model and mesh

The polynomial fitting of the thermophysical parameters of U78CrV rail steel with temperature is obtained:

$$\begin{cases} C_p = 7.75\times10^{-14}t^6 - 1.561\times10^{-10}t^5 + 1.156\times10^{-7}t^4 - 3.786\times10^{-5}t^3 + 5.765\times10^{-3}t^2 \\ -0.3142t + 497.2, (30 \le t \le 750) \\ C_p = -4.473\times10^{-5}t^3 + \ 0.1233t^2 + 113.4t + 3.54\times10^4, (750 < t \le 1000) \end{cases} \tag{11}$$

$$\begin{cases} \lambda = 4.69\times10^{-8}t^3 - 3.56\times10^{-5}t^2 - 5.701\times10^{-3}t + 34.62, (30 \le t \le 600) \\ \lambda = 3.505\times10^{-10}t^4 - 1.313\times10^{-6}t^3 + 1.862\times10^{-3}t^2 + 1.178t + 303.1, (600 < t \le 1000) \end{cases} \tag{12}$$

Given that: C_p and are λ specific heat capacity and thermal conductivity, respectively.

In this study, the transient heat transfer of a supersonic jet onto high-temperature rails is investigated, where variations in speed, pressure, and temperature occur dynamically in both time and space. The process is

characterized by diffusion, dissipation, and randomness [16], prompting the use of the Reynolds-averaged Navier-Stokes (RANS) equations for numerical simulation.

The near-wall region is modeled with the Enhanced Wall Treatment (EWT-e) function to accurately capture flow characteristics in close proximity to surfaces [17-19]. Boundary conditions are set as follows:

Outlet Boundary Condition: Standard conditions are applied at the outlet.

Wall Boundaries: These include the inner walls of the nozzle and the rail-jet interface. Non-slip wall boundary conditions are used, meaning flow velocities are set to zero (u=0, v=0, and w=0).

Gravity: Applied with an acceleration of -9.81kg/m^3 along the z-axis (negative sign indicating the direction).

To achieve a high accuracy of solution, second-order discretization is applied to the equations for energy, momentum, turbulent kinetic energy, and turbulent dissipation rate. The rail's initial temperature is set to 900°C, the nozzle inlet pressure is 0.3MPa, and the cooling period is defined at 100 seconds, providing the foundational conditions for analyzing the rail's cooling behavior under supersonic air flow.

3.2. Experimental verification

In order to facilitate processing, the SP nozzle is designed in a combined form: specifically, the nozzle is divided into two parts along the symmetrical surface in the width direction, and half of the cavity is machined separately and assembled into a whole with screws (as shown in Fig. 4). An "O" seal is used to secure the joint surface outside the nozzle cavity.

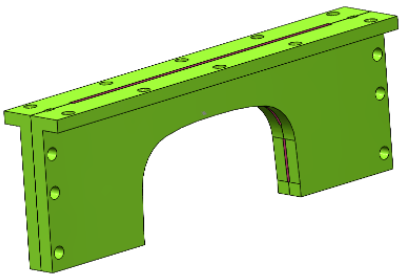

Fig. 4 Three-dimensional schematic diagram of SP nozzle

As shown in Fig. 5, screw drives are used to adjust the relative position of the rail and the nozzle in the X, Y, and Z directions. A SIRL2-2ML infrared thermometer was employed (measuring temperature range: 300-1300°C; spectral response: 1.6 μm; response time: 5 ms; repeated measurement accuracy: ±0.3%).

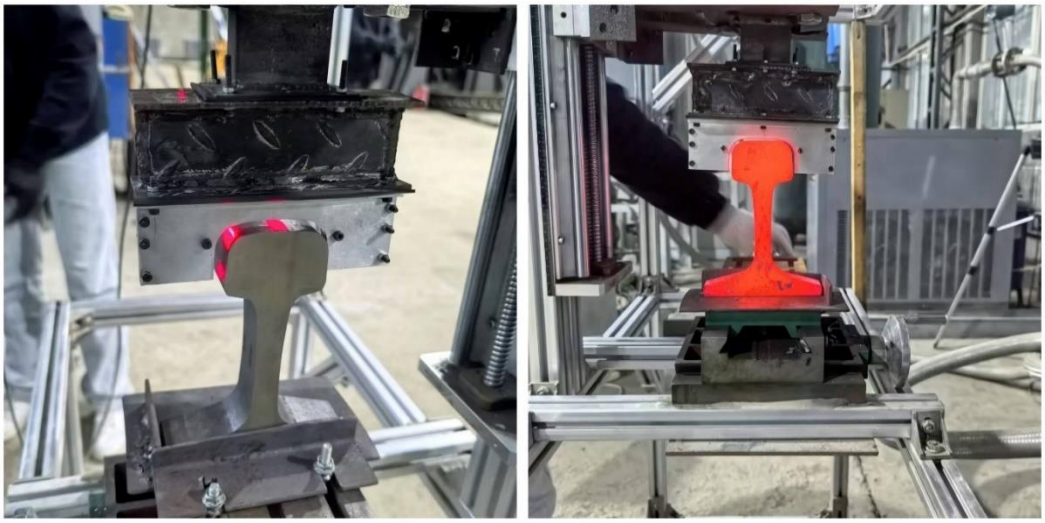

Fig. 5 Experimental device for air-cooled quenching of SP nozzle

The locations of the temperature test points (TP1, TP2, and TP3) are shown in Fig. 6. The "*" in the figure indicates the positions of the rail section hardness monitoring points required by China's railway industry standard "TB/T 2344.1-2020." The distance between the first point and the rail surface, as well as between the first point and the other points, is 5mm. Lines D and E are positioned 5 mm away from the lower jaw of the rail head; Line B is the bisector of Lines A and D; Line C is the bisector of Lines A and E.

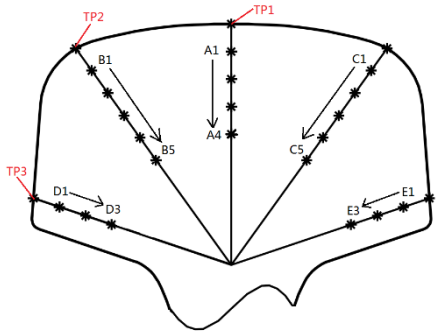

Fig. 6 Rail temperature test points

Fig. 7 shows the comparison between the experimental temperature measurements and the numerical simulation results, where RU represents the relative error, calculated as follows:

$$RU = \left| \frac{\text{Measured Value} - \text{Analogue Value}}{\text{Measured Value}} \right| \times 100\% \tag{14}$$

It can be observed that the numerical simulation results are in good agreement with the experimental results, with the maximum relative errors of TP1, TP2, and TP3 being 7.97%, 8.43%, and 8.50%, respectively, within the cooling duration of 100 seconds.

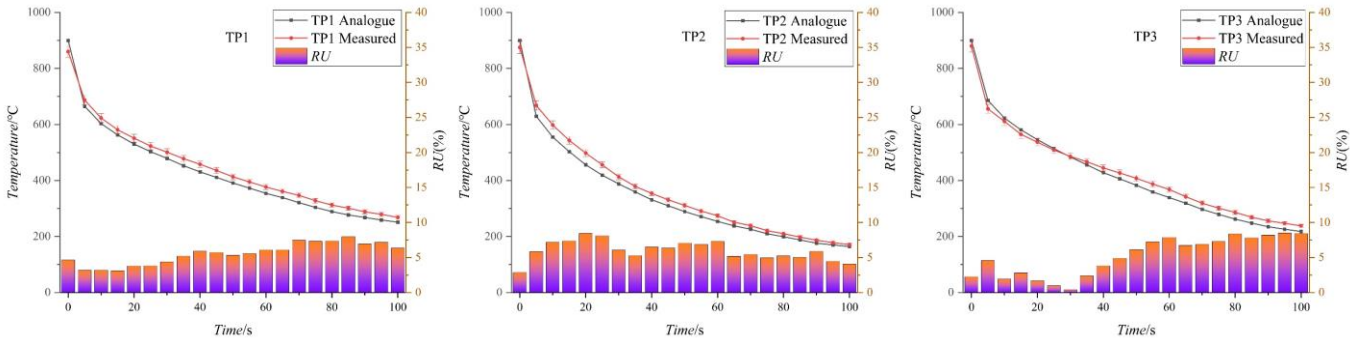

Fig. 7 Comparison of the measured temperature with the numerical simulation results

3.3. Results and Discussion

Fig. 8 shows the contours of the jet velocity field and pressure field of the SP nozzle after 100 seconds of cooling. It can be seen that when the compressed air reaches the throat position through the contraction section of the SP nozzle, the velocity significantly increases, approaching the speed of sound (approximately 340m/s) more uniformly. The fluid velocity of the airflow further increases when passing through the outlet expansion section, reaching supersonic speeds. The compressed air maintains a constant pressure at the inlet section of the nozzle, providing a continuous, stable inlet pressure. When the jet impacts near the surface of the rail, the speed decreases dramatically while the pressure increases.

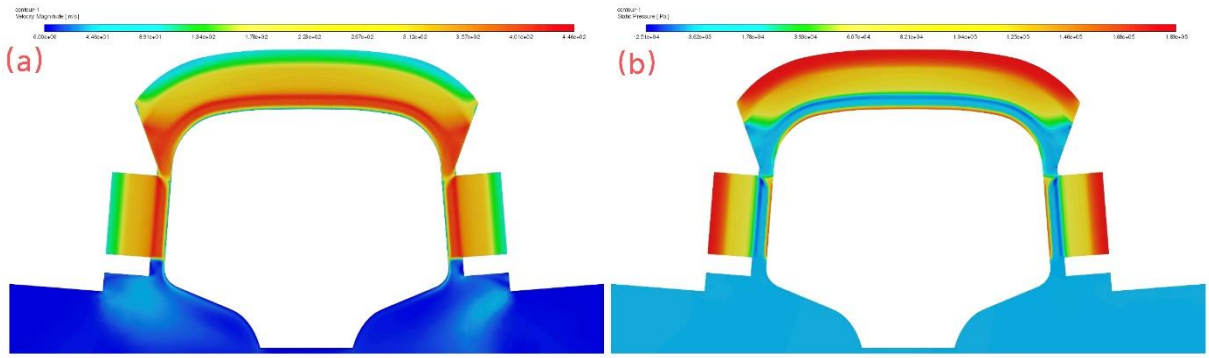

(a) Jet velocity field (b) Jet pressure field

Fig. 8 Jet flow field of SP nozzle

Fig. 9 presents a cross-sectional temperature diagram of the rail when the SP nozzle cools a 900°C rail for 100 seconds. It is evident that the temperature of the rail exhibits a decreasing distribution from the center of the rail head to the outer annulus. The low-temperature zone near the surface of the rail head is relatively uniform, and the temperature at the arc surface of the rail head is slightly lower than at other positions, indicating that the absence of a nozzle cavity in this area does not adversely affect the cooling effect on the rail.

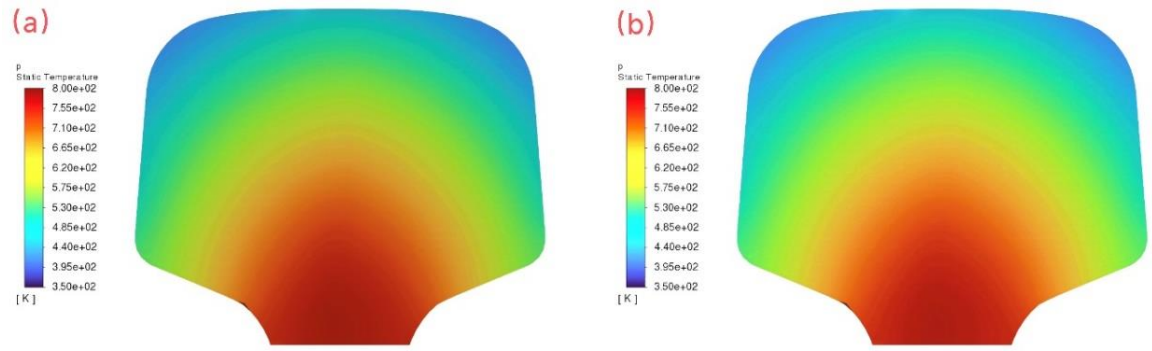

(a) Z=0 (b) Z=15

Fig. 9 Cross-sectional temperature contour of rail

Fig. 10 illustrates the cooling rates at various positions on the rail surface when the 900°C rail is cooled for 100 seconds using different types of nozzles at varying pressures. The CR nozzle, SR nozzle, and CP nozzle represent normal velocity shrink nozzles, supersonic round nozzles, and normal velocity profiling nozzles, respectively. The average cooling rate at each test point is used to characterize the nozzle's cooling capacity. The cooling capacity of the SP nozzle is significantly enhanced compared to the other types of nozzles. Specifically, the average cooling rate of the rail head increased by 26.82%, 7.64%, and 21.26% compared to the CR, SR, and CP nozzles, respectively, at a pressure of 0.13MPa. At 0.15MPa, the average cooling rate increased by 26.68%, 5.17%, and 21.72% compared to the same nozzles. The average cooling rate of the rail head was increased by 26.85%, 15.54%, and 19.95% compared to the CR, SR, and CP nozzles at a pressure of 0.3MPa. At 0.4MPa, the average cooling rates were enhanced by 23.96%, 15.35%, and 31.69%, respectively.

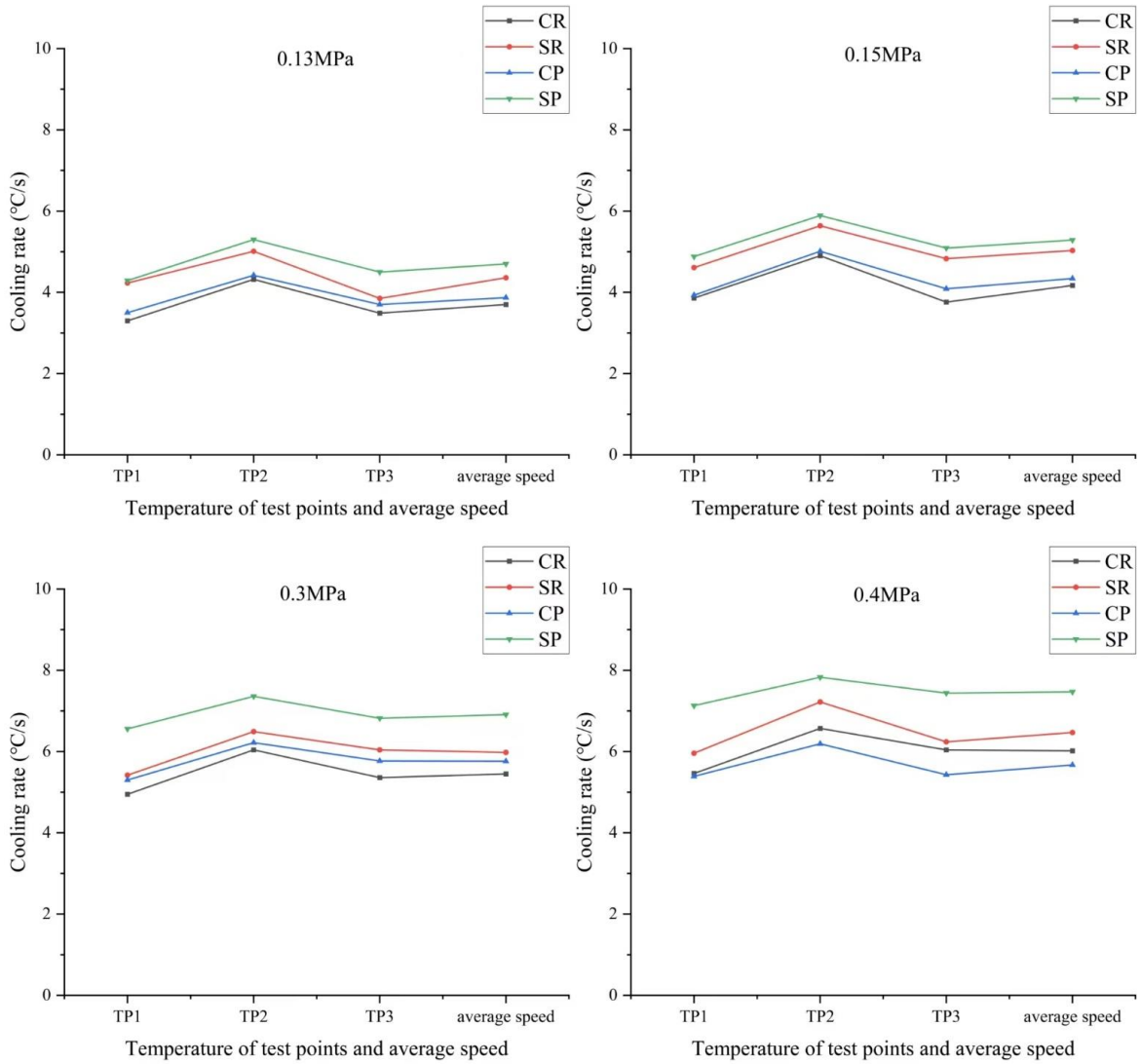

Fig. 10 Cooling rate of rail surface when different types of nozzles are used at different pressures

Fig. 11 displays the *Dev* values at different positions on the rail surface when cooling a 900°C rail for 100 seconds using various types of nozzles at different pressures. *Dev* is the standard deviation of the temperature at each test point, used to characterize the uniformity of the cooling rate across the rail head. The formula for *Dev* is as follows:

$$Dev = \sqrt{\frac{1}{n}\sum_{i=1}^{n}(X_i - \overline{X})^2} \tag{13}$$

where X_i is the cooling rate at the test point with the serial number *i*.

A smaller *Dev* value indicates less deviation from the average value and better uniformity in cooling across the test points on the rail head.

It is clear that the cooling uniformity of SP nozzles is significantly improved compared to other types. In terms of cooling uniformity, the *Dev* value for air-cooled quenching at a pressure of 0.13MPa decreased by

1.75%, 9.88%, and -10.14% compared to the CR, SR, and CP nozzles, respectively. After air-cooled quenching at 0.15MPa, the *Dev* value decreased by 15.58%, 1.75%, and 8.56% compared to the same nozzles. At 0.3MPa, the *Dev* value decreased by 25.88%, 24.04%, and 11.29%. At 0.4MPa, the *Dev* values decreased by 36.82%, 46.98%, and 22.19%, respectively.

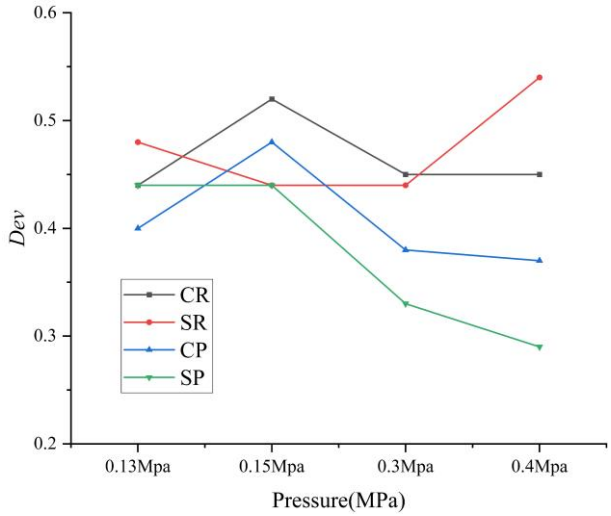

Fig. 11 Uniformity of cooling of rail surface when various types of nozzles are used at different pressures

A total of 15 temperature test points (TP1, TP2, TP3; A1, B1, D1; A2, B2, D2; A3, B3, D3; A4, B4, B5) are shown in Figure 6, with the average value of each set of 3 temperature test points taken as the temperature test layer (#TP, #1, #2, #3, #4). When the surface temperature is reduced to below the end temperature of the pearlite transition, the internal temperature may still remain within the pearlite transition temperature range. An increase in the surface cooling rate could cause the cooling rate below the surface to exceed V_c, resulting in the formation of martensite or bainite structures not permitted by the standard. This study designs a cooling process curve of "slow first and then fast," cooling at a rate close to but not exceeding V_c within the pearlite transition temperature range, followed by an increased cooling rate to minimize the longitudinal performance differences in the 100-meter rail and enhance production efficiency.

In previous studies, the critical cooling rate (V_c) for the U78CrV rail with an alloying element content of $[C]_{0.79}[Si]_{0.61}[Mn]_{0.79}[V]_{0.08}[Cr]_{0.31}$ was determined to be 3.6°C/s. Tab. 1 presents the average cooling rates of rail surface temperature test points (TP1, TP2, TP3) at different cooling stages and pressures. It is evident that within the phase transition temperature range (700-500°C), the average cooling rate of the rail head adjusts between 3.39-10.81°C/s, meeting the process requirements of the cooling rate range of 3-6°C/s for U78CrV rail steel during the phase change. However, at a jet pressure of 0.15MPa, the cooling rate exceeds 3.6°C/s. Consequently, when quenching the U78CrV rail with the SP nozzle, the inlet pressure during the phase transformation stage on the rail surface should be maintained at 0.13MPa.

Tab. 1 Average cooling rate of each test point on the rail surface at different pressures

Inlet pressure/MPa	Cooling phase/℃	Average cooling rate (℃/s)			
		TP1	TP2	TP3	$\bar{X}$
0.13	900-700	16.39	31.75	12.19	20.11
	700-500	3.37	3.56	3.24	3.39
	500-350	2.11	2.42	1.98	2.17
0.15	900-700	25	45.45	17.25	29.23
	700-500	3.68	6.45	4.16	4.76
	500-350	2.43	3.31	3.05	2.93
0.2	900-700	43.48	71.43	29.41	48.11
	700-500	5.52	9.90	5.88	7.10
	500-350	3.08	4.70	3.88	3.89
0.3	900-700	71.43	105.26	47.62	74.74
	700-500	8.62	14.92	8.89	10.81
	500-350	4.21	7.11	4.88	5.4

After numerous tests and simulations, it was finally determined that the pressure air cooling should initially be set at 0.13MPa for 90 seconds, followed by an increase to 0.15MPa for an additional 45 seconds. The cooling rates of each test layer of the rail at different cooling stages are shown in Tab. 2. At this point, the phase transformation of the rail is completed, and the cooling rates of each temperature test layer in the phase transformation temperature range (700-500°C) do not exceed the maximum cooling speed (V_c), thus meeting production requirements.

Tab. 2 Cooling rate of each test layer of the rail during different cooling stages

Inlet pressure/MPa	Cooling phase/℃	Average cooling rate (℃/s)				
		#TP	#1	#2	#3	#4
0.13	900-700	20.11	6.49	4.47	3.37	2.78
	700-500	3.39	3.44	3.00	2.87	2.75
	500-350	2.27				
0.15	900-700					
	700-500			3.59	3.56	3.52
	500-350	2.93	3.34	3.45	3.53	3.57

In the cooling stage after the phase change (500-350℃), the cooling rate of each test layer after the phase change of the rail at different pressures is shown in Tab. 3. After changing the inlet pressure, the average

cooling speed of the rail head can be adjusted to 2.51-5.81℃/s, the inlet pressure is 015MPa compared to 013MPa, 0.2MPa compared to 015MPa, 0.3MPa is 02MPa and 0.4MPa are better than The cooling rate of 3MPa has been increased by 0.85℃/s、0.59℃/s, 1.03℃/s and 0.83℃/s, the lifting rates were 33.86%, 17.56%, 26.08% and 16.67%, respectively.

Tab. 3 Cooling rate of each test layer after rail phase change at different pressures

Inlet pressure/MPa	Cooling phase/℃	Average cooling rate (℃/s)					
		#TP	#1	#2	#3	#4	$\bar{X}$
0.13		2.17	2.5	2.5	2.63	2.73	2.51
0.15		2.93	3.34	3.45	3.53	3.57	3.36
0.2	500-350			4.01	3.92	3.92	3.95
0.3				5.23	4.86	4.86	4.98
0.4				6.33	5.67	5.42	5.81

Fig. 12 shows the *Dev* curves of the rail surface test points using the SP nozzle at different inlet pressures. In the initial cooling stage, the inlet pressure significantly affects cooling uniformity, with *Dev* increasing notably as inlet pressure rises. As cooling progresses, the influence of inlet pressure on the uniformity of the cooling rate at different positions on the rail surface diminishes, with the *Dev* value tends to be the same at different inlet pressures when it is cooled to about 65 seconds. As cooling continues, the effect of jet pressure on *Dev* shows an inverse trend, where the *Dev* value decreases with increasing pressure, indicating improved cooling uniformity. After 90 seconds of cooling, the corresponding *Dev* values at jet pressures of 0.13MPa, 0.15MPa, 0.3MPa, and 0.4MPa were 0.48, 0.48, 0.47, and 0.39, respectively.

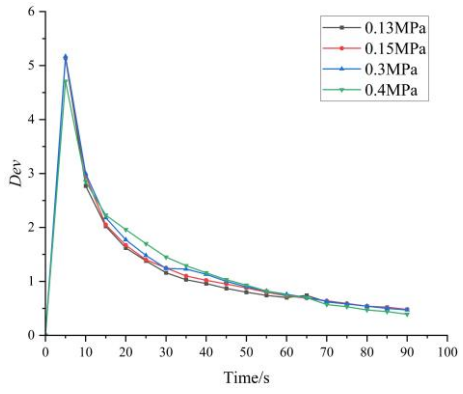

Fig.12 Dev curves of rail surface temperature using SP nozzle at different pressures

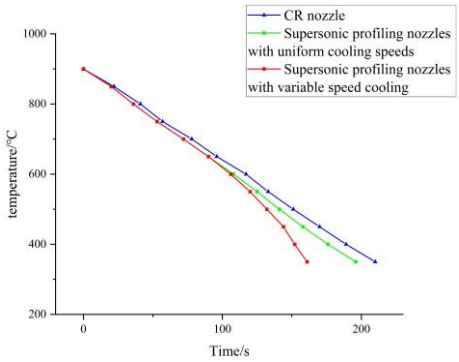

Fig.13 Cooling process curve

To sum up, this paper presents a cooling process curve characterized by a "slow first and then fast" approach. Initially, cooling occurs at a pressure of 0.13MPa for 90 seconds, followed by an increase to 0.15MPa for 45 seconds, and finally reaching a pressure of 0.4MPa until cooling is complete. Fig. 13 illustrates the cooling process curve. When the rail head temperature is reduced to 350°C, the times required for the CR nozzle, the supersonic profiling nozzle, and the segmented cooling supersonic profiling nozzle are 210 seconds, 196 seconds, and 161 seconds, respectively. Compared to the CR nozzles, the cooling time of the SP nozzle with segmented cooling is reduced by 49 seconds. Additionally, compared to the SP nozzle cooled at a constant rate, the cooling time is shortened by 35 seconds. During production, it is essential to adjust the inlet pressure of the SP nozzle so that the high-temperature steel is cooled at a rate close to, but not exceeding, the critical cooling rate for the pearlite transition before the rail reaches the end temperature of the pearlite transition (approximately 500°C) [20-21]. Subsequently, the nozzle inlet pressure should be increased as much as possible, as this approach enhances production efficiency while ensuring the performance of the heat-treated rail.

4. Conclusion

SP nozzles are designed and their cooling capacity and cooling uniformity are numerically investigated under different cooling parameters in this paper. The interesting findings have been gained:

(1) SP nozzle can significantly improve the cooling capacity and cooling uniformity of the rail, and carry out air-cooled quenching at a pressure of 0.4MPa, compared with the existing circular constant velocity nozzle, circular supersonic nozzle and constant velocity profiling nozzle, the cooling capacity is increased by 23.96%, 15.35% and 31.69% respectively. The cooling uniformity was increased by 36.82%, 46.98% and 22.19%, respectively.

(2) The inlet pressure has a significant impact on the cooling capacity of the SP nozzle, which increases with the increase of the inlet pressure. When the jet pressure increases from 0.13MPa to 0.15MPa, the cooling rate increases with the increase of pressure, and then decreases with the increase of pressure.

(3) Within the phase change temperature range (700-500°C), the average cooling speed of the rail head,

after adjusting the inlet pressure, is between 3.39-10.81°C/s. At a jet pressure of 0.15MPa, the cooling rate exceeds 3.6°C/s. Following extensive tests and simulations, the optimal cooling strategy was determined to involve starting at 0.13MPa for 90 seconds, then increasing to 0.15MPa for 45 seconds. At this point, the phase transformation of the rail is completed, and the cooling rates in the phase transformation temperature range (700-500°C) do not exceed the maximum cooling rate (V_c), thereby meeting production requirements.

(4) In the temperature range (500-350°C) following the phase change, the average cooling speed adjustment for the rail head varies between 2.51-5.81°C/s. At this stage, maximizing the nozzle inlet pressure is beneficial for improving production efficiency while ensuring the performance of the heat-treated rail.

(5) During the cooling initial stage, the uniformity of cooling from the SP nozzle is significantly affected by the inlet pressure, with the *Dev* value increasing as inlet pressure rises. As the rail temperature decreases, the influence of inlet pressure on cooling uniformity gradually diminishes. After approximately 65 seconds of cooling, the *Dev* values converge across different inlet pressures. As cooling continues, the effect of jet pressure on cooling uniformity reverses, with the *Dev* value decreasing as pressure increases.

(6) A segmented cooling process curve of "slow first and then fast" has been designed, resulting in a cooling time reduction of 49 seconds compared to the CR nozzle. Additionally, the cooling time is shortened by 35 seconds compared to the SP nozzle cooled at a constant rate. During production, it is essential to adjust the inlet pressure of the SP nozzle so that the high-temperature steel is cooled at a rate close to, but not exceeding, the critical cooling rate for the pearlite transition before the rail reaches the end temperature of the pearlite transition (approximately 500°C). Subsequently, the nozzle inlet pressure should be increased as much as possible, as this approach enhances production efficiency while ensuring the performance of the heat-treated rail.

Acknowledgements

This research was funded by the Liaoning Provincial Department of Education Service Local Project (2020FWDF11).

References

[1] Hu, J., *et al.*, Cause analysis of partial shelling on rail tread of high-speed railway, *Heat Treatment of Metals*, *44.S1*(2019), pp. 186-189.

[2] Wang, X., Research on the service life of rails and extension measures of the Da qin Railway, *China Railway*, *06*(2011), pp. 43-46.

[3] Ding, H., *et al.*, Effect of preheating/post-isothermal treatment temperature on microstructures and properties of cladding on U75V rail prepared by plasma cladding method, *Surface and Coatings Technology*, *399*(2020), pp. 126122.

[4] Gao, M., *et al*., Effect of Alloying Elements on Pearlite Critical Cooling Rate of U75V Rail-steel, T*ransactions of the Indian Institute of Metals, 76.3*(2022), pp 665-673.

[5] Li, B., *et al*., Dynamic CCT curve of U75V steel for high-speed railway, *Journal of Iron and Steel Research*, *26.11*(2014), pp. 20-24.

[6] Li, C., Online heat treatment of U75V rail, *Heat Treatment of Metals*, *43.01*(2018), pp. 152-156.

[7] Zhang, W., Study on bending deformation and residual stress of U75V heavy rail air-cooled quenching. D. thesis, Liaoning University of Science and Technology, Anshan, China, 2022.

[8] Gao, M., *et al*., Investigation the transient heat transfer to a supersonic air jet impinging on a high-temperature plate based on a discrimination-experiment method, *PLOS ONE*, *17.3*(2022), pp. 1-27.

[9] Song, L., Study on flow field and temperature field of U75V heavy rail supersonic air-cooled quenching. D. thesis, Liaoning University of Science and Technology, Anshan, China, 2021.

[10] Li, X., *et al*., Simulation of Temperature-field During Rail Air-cooling Quenching Process, *Journal of Wuhan University of Technology*, *34.7*(2012), pp. 146-148.

[11] Li, D., *et al*., Improvement of the Heat Treatment Process of U72Mn Steel Rail-Head, *Heat Treatment of Metals*, *29.12*(2004), pp. 65-68.

[12] Shan, Z., Design and study of 60kg/m heavy rail air-cooled quenching profiling nozzle. D. thesis, Liaoning University of Science and Technology, Anshan, China, 2022.

[13] Kang, H., Experimental study on key technologies of U75V heavy rail on-line heat treatment process. D. thesis, Northeastern University, Shenyang, China, 2012.

[14] Karimi, A. *et al*., Selective dehydration of high-pressure natural gas using supersonic nozzles, *Chemical Engineering & Processing Process Intensification*, *48.1*(2009), pp. 560-568.

[15] Xie, J., *et al*., Simulation Analysis of Supersonic Nozzle Discharge Coefficient, *Chinese Hydraulics & Pneumatics*, *46.12*(2022), pp. 123-128.

[16] Wu, J., Numerical simulation of U75V normalizing cooling process based on Fluent. D. thesis, Beijing Jiao Tong University, Beijing, China, 2021.

[17] S, S., *et al*., Application of a Reynolds-Stress Turbulence Model to the Compressible Shear Layer, *ICASE Report 90-18NASA CR*, 1990, pp. 182002.

[18] John, D., *Fundamentals of Computational Fluid Dynamics and Its Applications*, China Machine Press., Beijing, China, 2007.

[19] Yang, J., *et al*., Numerical study of transient conjugate heat transfer of the cryo-supersonic air-quenching based on a Mach-weighted pressure-based method, *International Journal of Heat and Mass Transfer*, *134*(2019), pp. 586-599.

[20] Kang, H., *et al*., Relationship between Rockwell hardness and pearlite lamellar spacing of hardened layer under different cooling rates for U75V 60kg/m heavy rail, *Materials Science & Engineering Technology*, *52.4*(2021), pp.460-467.

[21] Guo, D., *et al*., Laminar plasma jet surface hardening of the U75V rail steel: Insight into the hardening mechanism and control scheme-ScienceDirect, *Surface and Coatings Technology*, *394*(2020), pp. 125857.

Submitted: 11.11.2024
Revised: 07.01.2025
Accepted: 13.01.2025